Structural, electronic, and polarization properties of YN and LaN

A. J. E. Rowberg, S. Mu, M. W. Swift, and C. G. Van de Walle

Structural, electronic, and polarization properties of YN and LaN

A. J. E. Rowberg,[1] S. Mu,[1] M. W. Swift,[2, *] and C. G. Van de Walle[1, †]

[1]*Materials Department, University of California, Santa Barbara, CA 93106-5050, USA*
[2]*Center for Computational Materials Science, US Naval Research Laboratory, Washington, DC 20375, USA*

ScN has attracted great attention for its electronic properties and its ability to enhance polarization of AlN; however, its sister compounds, YN and LaN, remain much less-studied. Here, we use first-principles calculations to evaluate YN and LaN in their cubic and hexagonal phases. Rocksalt YN and LaN are semiconductors, although we show that LaN differs from ScN and YN in having a direct band gap, which we attribute to its weaker p-p coupling. Both have low electron effective masses. In addition to their rocksalt structures, we evaluate the layered hexagonal and wurtzite phases of YN and LaN. For YN, the wurtzite phase cannot be stabilized, and hexagonal YN is higher in energy than rocksalt YN. In contrast, for LaN, the wurtzite phase is favored, and it is comparable in energy to rocksalt LaN. Wurtzite LaN has a polarization of 0.608 C/m^2 (referenced to the centrosymmetric layered hexagonal phase), and a high piezoelectric coefficient $e_{33} = 1.78$ C/m^2. Interestingly, we find that the polarization of wurtzite LaN may be reversible; we find a relatively small switching barrier of 0.06 eV per formula unit, offering the potential for its use as a ferroelectric. Since wurtzite LaN is closely lattice matched to InP, we investigate a heterostructure between (0001) wurtzite LaN and (111) zincblende InP, and find the polarization discontinuity would yield a bound charge of 1.3×10^{14} e/cm^2, offering the potential for novel electronic applications such as tunnel junctions. Our results compare and contrast ScN, YN, and LaN, and highlight the potential of these materials for adoption in electronic and ferroelectric devices.

I. INTRODUCTION

Interest in scandium nitride (ScN) has recently surged,[1] adding it to the list of technologically important III-nitride compounds that includes GaN, AlN, and InN.[2] ScN is an indirect-gap semiconductor with high mobility,[3,4] promising thermoelectric properties,[5] high polarization discontinuities in heterostructures,[6] and ambipolar dopability.[7] While studies on ScN have flourished, two similar materials, yttrium nitride (YN) and lanthanum nitride (LaN), have barely been explored. Given their structural and chemical similarities, it seems plausible that these materials could offer similar or even superior functionality to ScN, possibly expanding the design space for semiconducting nitrides.

The first reports of the synthesis of YN and LaN date to the 1950s.[8,9] Their optical band gaps were measured almost two decades later, with values of 1.45 eV[10] and 1.5 eV[11] reported for YN and 0.82 eV for LaN.[10] Within the past 20 years, there have been intermittent attempts to synthesize thin films of YN through methods such as reactive laser ablation,[12] reactive sputtering,[13] and sublimation growth.[14] In each case, oxygen exposure was observed to affect film stability and conductivity,[12,14] leading to unintentional n-type conductivity, as is often seen in ScN.[1,4] However, Gregoire *et al.* demonstrated that a thin AlN protective layer significantly limited oxidation.[13] Experimental measurements[12–15] and computational reports[16–18] revealed that YN is indeed a semiconductor with an indirect band gap. In contrast, the nature of the fundamental band gap (indirect or direct) of LaN has remained under debate over the past twenty years. Limited theoretical studies on LaN have variously identified it as a metal,[19–21] an indirect-gap semiconductor,[16] or a direct-gap semiconductor.[22]

In fact, the suspected metallic nature of LaN was cited in the efficient catalytic performance of Ni-loaded LaN-surfaces for ammonia synthesis.[23]

Another potentially interesting aspect of these materials is their polarization. It has been observed that alloys of ScN and AlN result in an increased piezoelectric response relative to wurtzite AlN.[24] This is surprising, given that the ground-state structure of ScN is rocksalt, which is centrosymmetric. However, when adding modest amounts of ScN to AlN, the alloys retain the wurtzite structure. One might expect the alloy properties to be interpolated between wurtzite AlN and a metastable wurtzite ScN phase. However, when ScN is constrained to a hexagonal unit cell, it is not stable in the wurtzite structure (space group $P6_3mc$), but rather assumes a layered hexagonal structure (space group $P6_3/mmc$).[25] The enhanced piezoelectric polarization in Sc$_x$Al$_{1-x}$N alloys arises in spite of (or possibly *because of*[26]) the nonpolar nature of hexagonal ScN. Sc$_x$Al$_{1-x}$N alloys have also provided the first demonstration of switchable spontaneous polarization in III-nitrides.[27,28] Alloying ScN with AlN reduces the ferroelectric switching barrier.[26,29]

Y$_x$Al$_{1-x}$N alloys have also demonstrated enhanced piezoelectricity,[30,31] and in a hexagonal unit cell, YN also adopts the layered, nonpolar structure.[32] In a hexagonal unit cell, LaN, on the other hand, prefers the polar wurtzite crystal structure, with a total energy similar to that of the rocksalt phase.[19,20,22] To our knowledge, there are no previous studies that discuss the properties of the wurtzite phase. Wurtzite LaN exhibits a nonzero polarization, a feature that could be exploited in devices such as high electron mobility transistors (HEMTs). One experimental study has demonstrated the synthesis of wurtzite LaN (accompanied by the zincblende structure) in thin films using reactive sputter deposition.[33]

Identifying potential applications of YN and LaN requires a precise understanding of their structural and electronic properties. To that end, we perform accurate first-principles calculations based on density functional theory (DFT)[34,35] with a hybrid functional.[36,37] YN forms in the rocksalt structure; for LaN, we find the wurtzite structure to have a slightly lower energy than rocksalt. We confirmed this result by performing additional all-electron calculations using the full-potential linearized augmented plane-wave (LAPW) method.[38,39]

For the electronic structure of the rocksalt phases, we find that YN, like ScN, has an indirect band gap; however, rocksalt LaN has a direct band gap. We also determine the carrier effective masses at the band edges. The electron effective masses are similar to those of rocksalt ScN, which bodes well for n-type-conducting applications.

The finding that LaN can be stabilized in the wurtzite structure offers the prospect of exploiting its polarization properties. Its piezoelectric coefficient e_{33}=1.78 C/m^2 is larger than that of AlN. We find that it has a spontaneous polarization of 0.608 C/m^2 (referenced to the centrosymmetric layered structure), smaller than that of the other III-nitrides. The smaller value is related to its internal displacement parameter u being closer to 0.5 (the value in the hexagonal layered structure). This, in turn, offers the prospect of the polarization being switchable; indeed, our estimate for the switching barrier [0.06 eV per formula unit (eV/f.u.)] is smaller than the value similarly estimated for Sc$_x$Al$_{1-x}$N alloys, suggesting the possibility of ferroelectricity.

The paper is organized as follows. In Sec. II, we describe our computational methodology. Our results, in Sec. III, begin with an examination of the bulk properties and relative stability of different phases of YN and LaN (Sec. III A), with ScN included for comparison. In Sec. III B we discuss the electronic structure of the rocksalt phases, including their band structures (Sec. III B 1) and effective masses (Sec. III B 2). Section III C addresses the wurtzite phase of LaN, again focusing on its band structure (Sec. III C 1) and effective mass (Sec. III C 2), but also investigating its spontaneous (Sec. III C 3)and piezoelectric polarization (Sec. III C 5), the prospects for use in heterostructures (Sec. III C 4), and the ferroelectric switching barrier (Sec. III C 6). We summarize our findings in Sec. IV.

II. COMPUTATIONAL METHODS

We conduct first-principles calculations based on DFT[34,35] using the Heyd, Scuseria, and Ernzerhof (HSE)[36] screened hybrid functional, as implemented in the Vienna *Ab initio* Simulation Package (VASP).[40] Using the hybrid functional, in which the short-range exchange potential is calculated by mixing a fraction of nonlocal Hartree-Fock exchange with the generalized gradient approximation (GGA),[41] ensures a reliable descrip-

tion of the atomic and electronic structure, which is crucial for our present purposes. We use the default value of the mixing parameter, $\alpha = 0.25$, which yields a value of the direct band gap value for ScN within 0.1 eV of experimental measurements.[4,42] We therefore expect this choice to also offer reliable values for the gaps of YN and LaN, for which there is still experimental uncertainty.

We use an energy cutoff of 500 eV for the plane-wave basis set, and the core electrons are described with projector-augmented-wave (PAW) potentials,[43,44] with the Sc $3s^2$ $3p^6$ $4s^2$ $3d^1$, Y $4s^2$ $4p^6$ $5s^2$ $4d^1$, La $5s^2$ $5p^6$ $6s^2$ $5d^1$, and N $2s^2$ $2p^3$ electrons treated as valence. A 10×10×10 Γ-centered **k**-point mesh was used for the rocksalt structures, while an 8×8×6 mesh was used for the hexagonal structures (which have a larger real-space unit cell). Increasing the density of the **k**-point mesh affects energies by less than 0.2 meV/f.u. Structural relaxations were consistently performed using the hybrid functional. Total energies were converged to within 10^{-5} eV, and forces were considered converged when below 10 meV/Å.

For the rocksalt and wurtzite phases of LaN, all-electron DFT calculations were performed using the LAPW method as implemented in WIEN2k.[38,39] The muffin-tin radii were 2.46 bohr for La and 2.02 bohr for N. Energies were converged to within 5×10^{-5} Ry. The rocksalt lattice parameter was obtained by manually optimizing the volume to achieve a minimum total energy. The structural parameters for wurtzite were obtained by first manually optimizing the volume and the c/a ratio with fixed atomic positions, then relaxing the positions, and finally optimizing volume and c/a a second time. For both atomic and electronic structure calculations we used the Yukawa-screened PBE0 (YS-PBE0) hybrid functional[45] with parameters $\alpha_x = 0.25$ and $\lambda = 0.165$ bohr^{-1}, which have been shown to mimic HSE results accurately in a wide variety of compounds.[45] LAPW formation enthalpies were calculated based on DFT total energies for La metal and the isolated N atom together with the experimental atomization energy of molecular N$_2$.[46]

III. RESULTS AND DISCUSSION

A. Phase Stability

To begin, we calculate the lattice parameters and enthalpies of formation of YN and LaN in their pertinent phases. The four crystal structures we investigate are shown in Fig. 1. Two of the structures we consider have hexagonal unit cells: the layered hexagonal [Fig. 1(c)] and wurtzite [Fig. 1(d)] structures. Both zincblende [Fig. 1(b)] and wurtzite have tetrahedral coordination. In the wurtzite cell, atomic layers of cations and anions are offset by a certain amount along the c axis. The offset is quantified by the internal displacement parameter u, defined as the ratio of the cation–anion separation along the c axis to the c-lattice parameter. A wurtzite
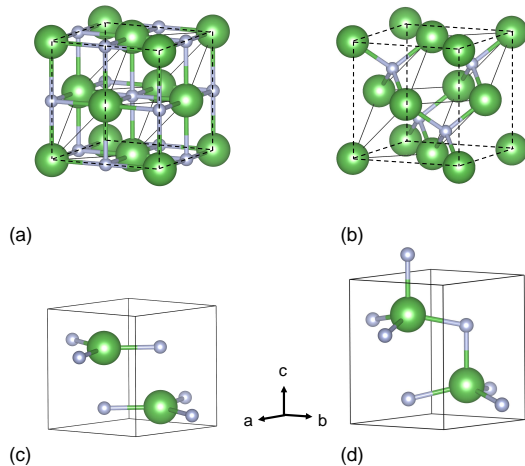
FIG. 1. Unit cells of crystal structures for (a) rocksalt (space group $Fm\bar{3}m$), (b) zincblende ($F\bar{4}3m$), (c) layered hexagonal ($P6_3mc$) with AA' stacking, and (d) wurtzite ($P6_3/mmc$). Nitrogen anions are indicated with small blue spheres, while cations are indicated with larger green spheres. The primitive unit cells are outlined by solid lines, while, for rocksalt and zincblende, the conventional cubic unit cell is shown by dashed lines. Structural images were generated with the VESTA3 software.[49]

structure with equal bond lengths in all directions would have $u=0.375$. Setting $u=0.5$ in the wurtzite unit cell recovers the layered hexagonal structure with AA' stacking [Fig. 1(c)], meaning that each cation is directly above and below nitrogen anions along the c axis in the nearest atomic layers. We have confirmed that another common configuration, AB stacking, is less favorable.

The lattice parameters and enthalpies of formation for these structures are summarized in Table I, alongside experimental values where available. We include values for ScN for comparison. Volumes are reported per f.u. These volumes increase monotonically from ScN to YN to LaN, and within each compound from the rocksalt to hexagonal/wurtzite phases. The rocksalt structures are between 13% and 16% smaller in volume than the hexagonal structures, consistent with the sixfold coordination (and hence greater density) in rocksalt. Our calculated structural properties agree quite well with experimental values, which are available for all rocksalt structures as well as for wurtzite and zincblende LaN. The layered hexagonal phase is dynamically stable for ScN and YN. We also investigated the layered hexagonal phase for LaN; however, we found it to be dynamically unstable, with small distortions leading it to adopt the wurtzite structure. We found the rocksalt structure of LaN to be dynamically unstable at $T=0$, in agreement with Chen *et al.*[22] Those authors found a distorted rocksalt phase with space group $P1$ to be lower in energy at $T=0$. We have confirmed their result with HSE, finding the $P1$ structure to be about 0.03 eV lower in energy than

the wurtzite structure. However, the $P1$ phase has not been experimentally observed, and Chen *et al.*[22] argued that finite-temperature effects will stabilize the higher-symmetry rocksalt structure; we therefore do not pursue further investigations of the $P1$ structure here.

The calculated formation enthalpies in Table I show that YN has a significant energetic preference for the rocksalt phase. The hexagonal phase is 0.20 eV/f.u. higher in energy. We found that YN cannot adopt the wurtzite phase; within the constraints of hexagonal symmetry, if we initialize the system in a wurtzite structure ($u < 0.5$), it spontaneously relaxes to the layered hexagonal structure ($u = 0.5$). This behavior was already reported in Ref. 32 and is very similar to that of ScN.[25] The instability of the wurtzite phase leads one to expect that the zincblende phase would not be stable, either: indeed, we find that the zincblende structures possess soft phonon modes that render them dynamically unstable. In addition, our calculations for the (symmetry-constrained) zincblende phase show that it is much higher in energy than the rocksalt phase: by 0.86 eV/f.u. for ScN and by 0.57 eV/f.u. for YN.

The situation is different for LaN, for which the wurtzite structure can be stabilized. The formation enthalpies of rocksalt and wurtzite LaN are very similar within the error bar of the calculations (Table I). To verify the accuracy of this result, and in particular, to make sure it is not affected by our PAW methodology, we conducted all-electron calculations within the LAPW formalism, as outlined in Sec. II. The two approaches produce similar values for the structural parameters (Table I), including for the internal displacement parameter u of wurtzite LaN, which is $u=0.414$ in PAW and $u=0.413$ in LAPW. The difference in formation enthalpies between rocksalt and wurtzite is very similar in the PAW and LAPW approaches, with both showing a small energetic preference for the wurtzite structure. The values of the formation enthalpies themselves differ by about 0.1 eV when comparing PAW and LAPW; the difference can be directly attributed to the method for calculating these enthalpies. The LAPW values use an experimental atomization energy, while the HSE values calculate molecular N_2 directly. If we instead calculate enthalpies in the same manner (i.e., using atomic N and the experimental atomization energy), the HSE values are in near-perfect agreement with those of the LAPW method. Both our own work and the calculations of Ref. 22 show the wurtzite phase to be dynamically stable. We conclude that, given the right synthesis conditions, stabilizing LaN in the wurtzite crystal structure should be possible, as has recently been demonstrated experimentally.[33] The experimental work found the zincblende phase to coexist with the wurtzite phase. Our calculations for the zincblende phase of LaN actually find it to be dynamically unstable, with soft phonon modes; stabilization may occur due to the surrounding wurtzite matrix. Since the zincblende phase has been experimentally observed, and since it is only 0.14 eV higher in energy than the wurtzite

TABLE I. Calculated and experimental bulk properties for the rocksalt (rs), layered hexagonal (hex), wurtzite (wz), and zincblende (zb) phases of ScN, YN, and LaN. For LaN, all-electron LAPW results obtained with WIEN2k are listed alongside PAW results obtained with VASP.

Structure	Method	a (Å)	c (Å)	Vol per f.u. (Å^3)	E_g^{ind} (eV)	E_g^{dir} (eV)	ΔH^f (eV/f.u.)
rs-ScN	VASP	4.48	–	22.47	0.88	1.99	−4.20
	Exp.	4.51[a]	–	22.78	0.9±0.1[b]	2.02[c]	–
hex-ScN	VASP	3.71	4.48	26.81	1.50	2.34	−3.97
rs-YN	VASP	4.88	–	29.01	1.08	1.55	−3.80
	Exp.	4.88[d]	–	29.04	–	1.45[e]–2.3[f]	–
hex-YN	VASP	4.01	4.88	33.93	1.69	1.98	−3.60
rs-LaN	VASP	5.28	–	36.86	1.06	0.76	−2.60
	WIEN2k	5.32	–	37.68	1.17	0.95	−2.49
	Exp.	5.30[g]	–	37.21	–	0.82[h]	–
wz-LaN	VASP	4.12	5.91	42.47	2.29	2.47	−2.61
	WIEN2k	4.15	5.98	44.70	2.35	2.63	−2.51
	Exp.[i]	4.08	5.84	42.10	–	–	–
zb-LaN	VASP	5.59	–	43.65	2.41	2.19	−2.47
	Exp.[i]	5.60	–	43.90	–	–	–

[a]Ref 47; [b]Ref 48; [c]Ref 4; [d]Ref 8; [e]Ref 10; [f]Ref 13; [g]Ref 9; [h]Ref 10; [i]Ref 33

phase, we include our calculated properties for zincblende LaN in Table I.

The preference of LaN for the wurtzite phase is contrary to what we and others have found for hexagonal ScN[25] and YN[32], both of which prefer layered hexagonal structures with an internal displacement parameter of u=0.5, in which cations and anions are coplanar. However, the value of the internal displacement parameter in wurtzite LaN, u=0.414, is significantly larger than in conventional nitride semiconductors such as AlN (u=0.382), GaN (u=0.377), and InN (u=0.380).[50] The fact that u is closer to 0.5 in LaN indicates the material might lend itself to ferroelectric switching, which requires moving layers of anions and cations relative to each other and overcoming a barrier that occurs at the centrosymmetric structure corresponding to u=0.5. We will return to this topic, and more generally discuss polarization, in Sections III C 3 and III C 6.

B. Rocksalt Phase

1. Band Structures

Figure 2 displays the HSE band structures for ScN, YN, and LaN; we include ScN for purposes of comparison. The band-structure plots are positioned side-by-side with plots of the orbital-projected density of states (DOS), with contributions from different atomic orbitals indicated by different colors.

Qualitatively, the band structures of all three compounds are quite similar; the main difference is that the highest valence band at X rises in energy relative to Γ in going from Sc to Y to La. The indirect band gaps occur between the valence-band maximum (VBM) at Γ and the conduction-band minimum (CBM) at X, and are similar in magnitude in all three compounds (values listed in Table I), with ScN having a slightly smaller indirect gap than YN and LaN. Because of the rising valence band at X, the direct band gap (also listed in Table I) distinctly decreases. Both ScN and YN have indirect gaps, but the band gap in LaN becomes direct at the X point and smaller in magnitude than the indirect band gap by 0.4 eV. LaN thus differs qualitatively from ScN and YN. The direct nature of the band gap has only recently been recognized;[22] calculations based on lower levels of theory identified LaN as a metal or an indirect-gap semiconductor.[16,19,21] The highest valence band at Γ is three-fold degenerate (in the absence of spin-orbit coupling). In ScN and YN, the highest VB at X is doubly degenerate, and a singly degenerate band is 2.47 eV lower in energy in ScN, and 1.31 eV lower in energy in YN. In LaN, the VBM at X is non-degenerate, resulting from the singly degenerate band pushing 0.05 eV above the twofold degenerate band. This change is also reflected in the bandwidths corresponding to the highest three valence bands, which decrease across the three materials as the cation size increases, from 5.67 eV in ScN to 4.51 eV in YN and 3.27 eV in LaN.

Our calculated orbital-projected DOS, shown alongside the band structures in Fig. 2, help to explain these observations, along with an inspection of the character of the states at the X point. The valence band at X is
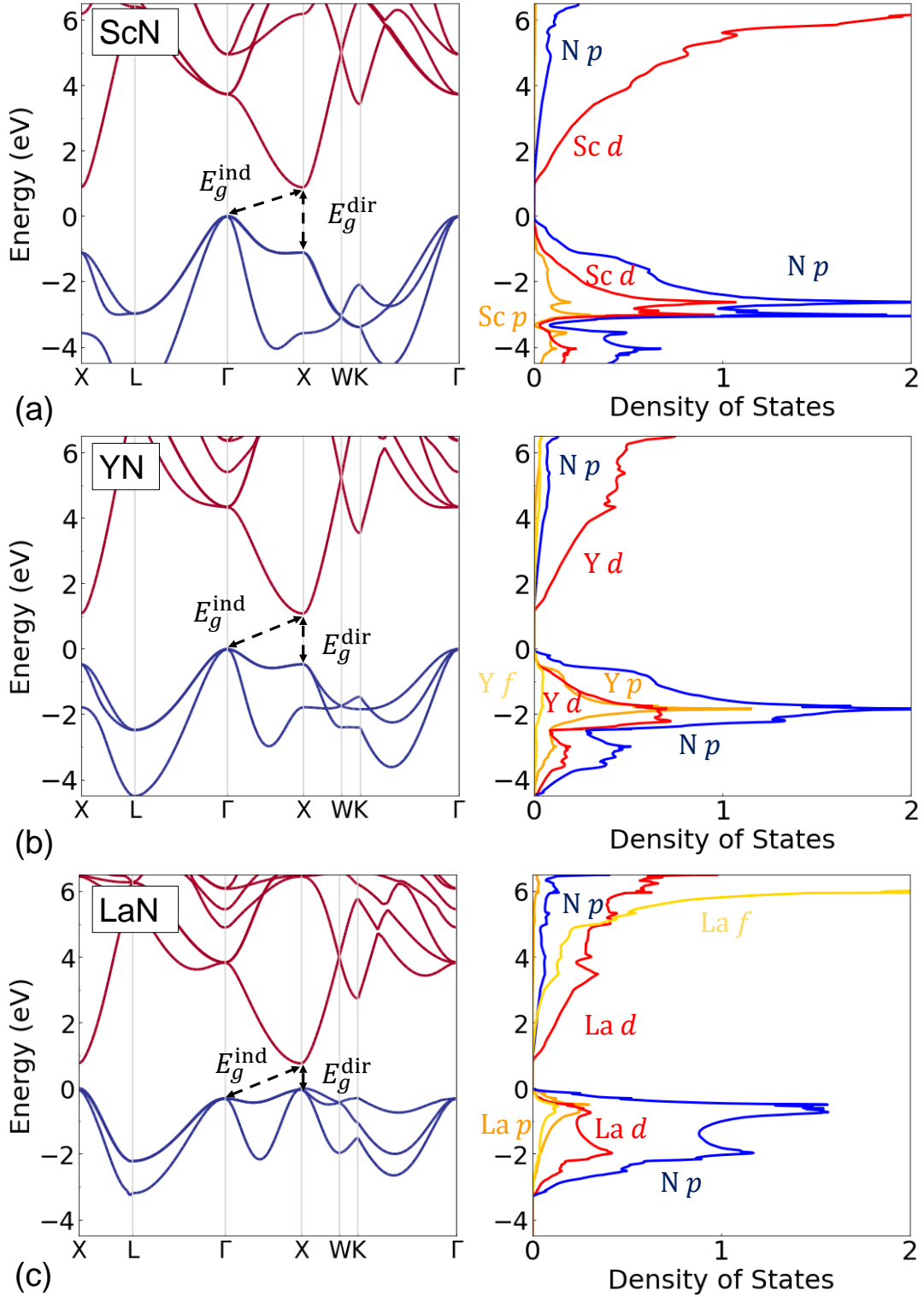
FIG. 2. Band structures, as calculated with the HSE hybrid functional, alongside densities of states for (a) ScN, (b) YN, and (c) LaN in their rocksalt crystal structures. The indirect and direct band gaps are indicated, as are the specific atomic orbitals contributing to the orbital-projected densities of states. The zero of energy is set at the valence-band maximum.

dominated by N $2p$ character, but cation p orbitals play a sizeable role; cation d orbitals, on the other hand, have little weight at the X point. The interaction between anion and cation p states explains the sizeable splitting between the valence bands at X in the case of Sc and Y. The one-fold degenerate valence band at X arises from σ bonding between cation and N p states, while the two-fold degenerate state arises from (weak) π bonding. As the size of the cation increases, the strength of the σ bond decreases, raising the energy of the nondegenerate band, until the splitting between the valence bands at X essentially disappears in the case of LaN.

2. Effective Masses

The effective-mass tensor is defined as:

$$\left[\frac{1}{m_{\mathbf{k}}^*}\right]_{ij} = \frac{1}{\hbar^2}\frac{\partial^2 \varepsilon_{\mathbf{k}}}{\partial k_i \partial k_j} \ . \tag{1}$$

We determined the effective masses by a parabolic fit close to the band extrema.

In Table II, we list effective masses for electrons in the CBM at X in the transverse and longitudinal directions. In the rocksalt Brillouin zone (BZ), at the X high-symmetry point, the longitudinal direction is oriented along the pathway X$\rightarrow\Gamma$, while the transverse direction is X $\rightarrow$ W. As a means to connect the effective mass with values that can be measured experimentally, we calculate transport effective masses m_{tr} and density-of-states effective masses m_{DOS}. These are defined as

$$m_{\text{cond}} = 3\left(\frac{1}{m_l} + \frac{2}{m_t}\right) \tag{2}$$

and

$$m_{\text{DOS}} = (m_l m_t^2)^{1/3}, \tag{3}$$

where m_l is the longitudinal effective mass and m_t is the transverse effective mass. For the density-of-states effective mass, we note that our definition does not include the factor $M_c^{2/3}$, where M_c is the number of equivalent band minima ($M_c = 3$ for the CBM in ScN, YN and LaN).[51] Table II includes values for ScN for comparison;[42] as can be seen, the effective masses for YN and LaN are comparable to those of ScN, suggesting that they, too, may have utility as n-type conductors.

Table III lists effective masses for holes for the three highest valence bands (VB1, VB2, and VB3), again with previously calculated values for ScN included for comparison.[42] The masses are distinctly anisotropic. In ScN and YN, the highest-lying valence bands VB1/VB2 are heavy-hole bands, and VB3 is the light-hole band. At the X point in LaN, the order of heavy-hole and light-hole band switches when going from X $\rightarrow$ Γ to X $\rightarrow$ W.

TABLE II. Effective masses for electrons (in units of the electron mass m_0) at the CBM in rocksalt (rs) ScN (from Ref. 42), YN, and LaN: longitudinal mass m_l, transverse mass m_t, transport mass m_{tr}, and density-of-states effective mass m_{DOS}.

Compound	m_l	m_t	m_{tr}	m_{DOS}
rs-ScN	1.43	0.17	0.24	0.34
rs-YN	1.17	0.16	0.22	0.31
rs-LaN	1.20	0.18	0.25	0.34

TABLE III. Effective masses for holes (in units of the electron mass m_0) at the VBM, which is at Γ in rocksalt (rs) ScN and YN, and at X in LaN. Values for rs-ScN from Ref. 42. The X $\rightarrow$ Γ and X $\rightarrow$ W directions correspond to longitudinal and transverse directions, respectively.

Compound	Valence band	m_h ($\Gamma \rightarrow$ X)	m_h ($\Gamma \rightarrow$ L)
rs-ScN	VB1/VB2	0.74	0.40
	VB3	0.15	0.24
rs-YN	VB1/VB2	0.99	0.43
	VB3	0.16	0.25
		m_h (X $\rightarrow$ Γ)	m_h (X $\rightarrow$ W)
rs-LaN	VB1	0.27	1.78
	VB2/VB3	2.07	0.30

C. Wurtzite Phase

As discussed in Sec. III A, only LaN can be stabilized in the wurtzite structure, so this section will be focused on this compound.

1. Band Structure

The calculated band structure of wurtzite LaN is depicted in Fig. 3, alongside its orbital-projected DOS. It has a significantly wider band gap than rocksalt LaN. The band gap is indirect, with the VBM at K and the CBM at Γ. The direct gap at K is only 0.18 eV higher in energy (see Table I). Such a "quasi-direct" band structure can be favorable for applications such as in photovoltaics, since strong optical absorption will occur at energies only slightly above the fundamental gap, while radiative recombination is suppressed. The VBM is comprised predominantly of N p states, while the CBM has mostly La d character, similar to rocksalt LaN [Fig. 2(c)]. The bands are singly degenerate at both the VBM and the CBM. The band gap of wurtzite LaN is considerably larger than that of the rocksalt phase: this difference is consistent with stronger bonding, which follows from the lower coordination (fourfold in wurtzite, sixfold in

TABLE IV. Effective masses for electrons and holes (in units of the electron mass m_0) along high-symmetry directions in wz-LaN.

Compound	m_e $(\Gamma \rightarrow \text{K})$	m_e $(\Gamma \rightarrow \text{A})$	m_h $(\text{K} \rightarrow \text{M})$	m_h $(\text{K} \rightarrow \Gamma)$
wz-LaN	0.08	0.35	2.32	0.67

rocksalt) and shorter La–N bond lengths (2.43–2.45 Å in wurtzite, 2.66 Å in rocksalt).

2. Effective Masses

We list the effective masses at the band extrema in wurtzite LaN in Table IV. The electron mass at Γ is quite small but highly anisotropic. Hole effective masses are larger.

3. Spontaneous polarization

We calculate the formal polarization along the c axis of wurtzite LaN according to the modern theory of polarization:[52,53]

$$\mathbf{P}_f = \frac{e}{\Omega} \sum_s Z_s \mathbf{R}_s - \frac{ief}{8\pi^3} \sum_j \int_{\text{BZ}} d\mathbf{k} \langle u_{j,\mathbf{k}} | \nabla_{\mathbf{k}} | u_{j,\mathbf{k}} \rangle. \quad (4)$$

The first term, corresponding to the ionic contribution, sums over all atomic positions $\mathbf{R}_s$ in the unit cell, multiplying by the ionic charges Z_s and the charge of the electron e, and dividing by the unit cell volume Ω. The second term describes the electronic contribution, obtained through a summation over all occupied bands j and integration over the BZ. f refers to the spin degeneracy of the bands, and $\langle u_{j,\mathbf{k}} | \nabla_{\mathbf{k}} | u_{j,\mathbf{k}} \rangle$ is the Berry potential.[52,53] $\mathbf{P}_f$ is only defined modulo the quantum of polarization.

We follow the procedure outlined in Ref. 50. Physical values of spontaneous polarization are defined as a difference of formal polarizations between the structure of interest and a reference structure; we choose that reference to be the layered hexagonal structure (with $u=0.5$), which is centrosymmetric and has zero formal polarization. We start from the optimized structure for the wurtzite phase, keep the lattice parameters fixed, and construct an array of interpolated structures with fixed lattice parameters but different internal displacement parameters u, ranging from $u=0.414$ for wurtzite to $u=0.5$ for the layered hexagonal phase. This procedure ensures we stay on a specific branch of the multivalued polarization. The resulting values of polarization as a function of u are plotted in Fig. 4, expressed in units e/A, where A is the unit-cell area in the plane perpendicular to c $[A = (\sqrt{3}/2)a^2]$; A=14.716 Å^2 in wurtzite LaN.

This procedure leads to a value of the spontaneous polarization in LaN of P_{sp}=0.559 e/A = 0.608 C/m^2. Ex-

pressed in units C/m^2, this value is less than half that of GaN (1.312 C/m^2).[50] There are two reasons for this difference. First, the larger u value of LaN leads to a smaller polarization because the crystal is closer to the nonpolar, layered hexagonal (u=0.5) structure. Second, the in-plane lattice parameter, a=4.122 Å, of LaN is significantly larger than in GaN. Since polarization is generated by a dipole within the unit cell, and since the charges in that dipole are roughly the same for any III-V compound, we expect the polarization to scale inversely with the in-plane area of the unit cell.

This point is well illustrated by expressing the polarization in units of e/A, as we do in Fig. 4. Figure 4 includes values for AlN, GaN, and InN from Dreyer et al.[50] It is clear that in units of e/A, the curves for AlN, GaN, and InN essentially coincide, and the different polarizations in the compounds are then solely due to the difference in u values. For GaN, where A=8.896 Å^2, the polarization at the equilibrium value of u=0.377 is 0.727 e/A. Taking the polarization of GaN (at u=0.377) and using interpolation to determine the polarization that would result for $u = 0.414$, we find a value of 0.509 e/A, which is within 10% of the actual calculated value (0.559 e/A) for LaN. When expressed in units of e/A, the difference in u values in GaN and LaN clearly accounts for the majority of the difference in spontaneous polarization. Still, Fig. 4 makes clear that the polarization of LaN is not on the same trend line as those of AlN, GaN, and InN. We attribute this to the fact that bonding in LaN does not consist of simple sp bonding, but involves d states; the resulting distortion in the electron distribution clearly has some impact on the calculated polarization.

4. Heterostructure design

We can use our calculated values of polarization to predict polarization differences at interfaces. In conventional III-nitrides, such polarization discontinuities are exploited at GaN/AlGaN interfaces to enhance the density of the two-dimensional electron gas in HEMTs; the bound charge at such interfaces is on the order of a few times 10^{13} e/cm^2.[50] In order for the spontaneous polarization in LaN to be used in this fashion, a suitable heterojunction with another semiconductor needs to be identified, which should exhibit a good structural match. The conventional wurtzite III-nitrides (AlN, GaN, and InN) are not good candidates due to their large lattice mismatch with the larger LaN. We can also consider materials that assume the zincblende crystal structure [Fig. 1(b)], which is characterized by ABC stacking along the (111) direction, offering a direct match to the AB stacking of wurtzite along the c axis [Fig. 1(d)]. Epitaxial growth of wurtzite LaN on a (111) zincblende substrate should therefore be feasible if a material with reasonable lattice match can be identified; this would require a cubic lattice parameter close to $a_{wz}\sqrt{2}$ =5.830 Å.

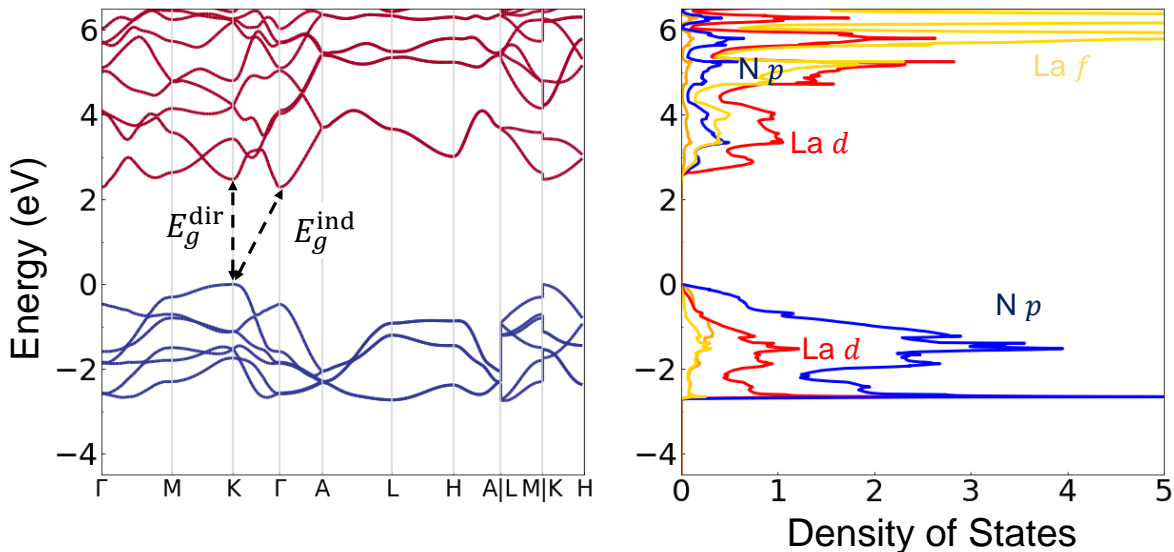One material that fits this description is InP, which has

FIG. 3. Band structure and orbital-projected density of states for wurtzite LaN, with the direct and indirect band gaps indicated. The zero of energy is set at the VBM.
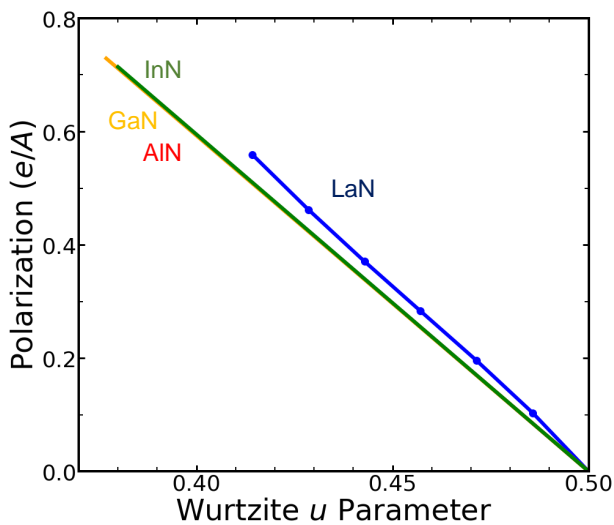

FIG. 4. (a) Polarization (in units of e/A) as a function of u in LaN, InN, GaN, and AlN. Data for InN, GaN, and AlN are adapted from Ref. 50.

a lattice parameter of 5.87 Å.[54] III-V zincblende materials have a polarization of 0.750 e/A along the [111] axis;[50] thus, the polarization difference between wurtzite LaN and zincblende InP would be $0.750 - 0.559 = 0.191$ e/A. The bound charge at this heterostructure would therefore be 0.205 C/m^2, or approximately 1.3×10^{14} e/cm^2, considerably larger than at GaN/AlGaN interfaces.[50] In addition to applications in HEMTs, large polarization discontinuities may be useful for tunnel junctions or to generate high-density carrier gases for contacts or current-spreading layers.

As an additional note, we observe that the *rocksalt* structures of YN and LaN may also have applications in heterostructures with wurtzite materials,[55] similar to the case of interfaces between rocksalt ScN and wurtzite GaN discussed in Ref. 6. Such heterojunctions offer large polarization discontinuities that can be exploited in similar devices as discussed above. Rocksalt YN and LaN have the same formal polarization as rocksalt ScN ($3/2$ e/A), and they should behave in much the same fashion as rocksalt ScN when integrated with a wurtzite III-V compound.[6]

5. *Piezoelectric polarization*

We also compute the piezoelectric constants, e_{ij}, of wurtzite LaN. These constants can be decomposed into clamped-ion and internal-strain contributions:[56]

$$e_{ij} = e_{ij}^{\text{clamped}} + e_{ij}^{\text{int}}$$
$$= \left.\frac{\partial P_i}{\partial \varepsilon_j}\right|_u + \sum_{\alpha,k} \left.\frac{\partial P_i}{\partial u_{\alpha,k}}\right|_\varepsilon \frac{\partial u_{\alpha,k}}{\partial \varepsilon_j} . \tag{5}$$

P_i is the polarization along the i direction, and ε_j is the strain along the j direction. The j values are expressed in Voigt notation, with $j = 1$ corresponding to xx, $j = 2$ to yy, $j = 3$ to zz, $j = 4$ to yz, $j = 5$ to zx, and $j = 6$ to xy. $u_{\alpha,k}$ is the internal atomic coordinate along the k direction for atom α in the wurtzite unit cell. We note that the $u_{\alpha,k}$ values are related to the internal displacement parameter u by $u = u_{\text{La},3} - u_{\text{N},3}$. The clamped-ion term e_{ij}^{clamped} arises from the contributions of electrons when the ions are clamped at their zero-strain equilibrium internal atomic coordinates $u_{\alpha,k}$; i.e., the ionic coordinates

follow the strain-induced deformation of the lattice vectors. The internal-strain contribution e_{ij}^{int}, on the other hand, reflects the change in polarization arising from the distortion of ionic coordinates at fixed strain.

In the wurtzite structure, strain both along and perpendicular to the c axis can give rise to polarization along the c axis, corresponding to the piezoelectric coefficients e_{33} and e_{31} (by symmetry, $e_{32}{=}e_{31}$).

Our calculated values are $e_{33}{=}1.78$ C/m^2 and $e_{31}{=}{-}0.12$ C/m^2. The e_{33} value is significantly larger than those of conventional III-nitrides [e_{33}(AlN)=1.57 C/m^2, e_{33}(GaN)=1.02 C/m^2, and e_{33}(InN)=1.24 C/m^2, Ref. 50], which could be very technologically useful.

A decomposition of the piezoelectric coefficient yields $e_{33}^{\text{clamped}} = -0.64$ and $e_{33}^{\text{int}}= 2.42$ C/m^2, demonstrating that internal-strain contributions dominate. For e_{31}, we found competing contributions from the internal-strain term (-0.33 C/m^2) and the clamped-ion term (0.21 C/m^2).

6. Ferroelectric switching

LaN's large u parameter renders it potentially suitable as a ferroelectric, which requires switching the polarization under an applied electric field. Polarization switching would be achieved by moving the La atoms in the direction of the N atoms, increasing the u value until the La atoms arrive at their symmetrically equivalent position on the opposite side of the N atomic plane (at $1{-}u$). The barrier for this process occurs at $u = 0.5$, i.e., the centrosymmetric layered hexagonal structure. In AlN, GaN, and InN, u is close to the ideal value of 0.375, and the atomic positions are too far from the centrosymmetric structure to permit switching. The larger u value in LaN should make switching (between $u = 0.414$ with $P_{sp} = 0.608$ C/m^2 and $u = 0.586$ with $P_{sp} = -0.608$ C/m^2) more feasible.

To examine the potential for ferroelectric switching, we use the solid-state nudged elastic band (ss-NEB) method[57] to determine the energy of intermediate structures that would occur during switching. We then determine the polarization at these intermediate structures, and plot the energy as a function of polarization in Fig. 5 (solid blue dots). The ss-NEB method requires that the initial and final images are energetic minima; thus, we are restricted to data points in the range shown. We fit these data to a fourth-order polynomial, in the spirit of Landau-Ginzburg theory:[58]

$$E(P) = E_0 + \frac{1}{2}aP^2 + \frac{1}{4}bP^4 , \qquad (6)$$

where E_0 is the energy of the centrosymmetric, nonpolar structure and a and b are fitting parameters. The plot shows two stable positions, corresponding to the equivalent configurations with opposite polarization at $u = 0.414$ and $u = 0.586$; these energetic wells are separated by a saddle point corresponding to the hexagonal
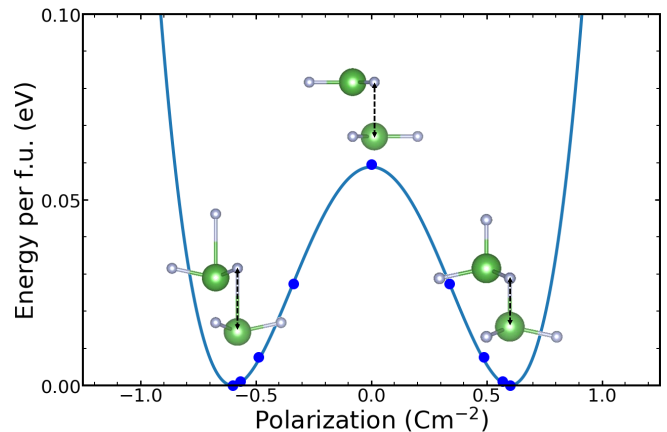

FIG. 5. Energy per formula unit, referenced to the lowest-energy structures, as a function of polarization in wurtzite LaN, obtained from ss-NEB calculations. The insets show the ground-state structure ($u = 0.414$) along with the hexagonal ($u = 0.500$) and inverted wurtzite ($u = 0.586$) structures. The blue line is a fit to a fourth-order polynomial, using the data points indicated with blue dots.

$u = 0.5$ structure. We find the switching barrier to be 0.06 eV/f.u.

We note that in ss-NEB calculations, both the atomic positions and volume are relaxed for each image. Allowing volume relaxation allows the configuration with $u = 0.5$ to reach its lowest energy, which permits a more accurate estimation of the barrier. We find that in going from $u = 0.414$ to $u = 0.5$ the volume contracts by 2.2%, driven by a 9.4% contraction of the c lattice parameter. If we were to freeze the lattice parameters to those of the equilibrium wurtzite phase and evaluate the energy as a function of the u parameter, we would obtain a much larger switching barrier, namely 0.21 eV/f.u.

The barrier calculated here is only an estimate of the actual barrier. In real systems, ferroelectric switching involves initial nucleation of a reversed domain followed by gradual switching of the global polarization via domain-wall motion. This domain-wall motion is not captured in our ss-NEB calculation, which uses a four-atom unit cell and assumes a simultaneous and uniform switching of the entire dipole, potentially overestimating the switching barrier. On the other hand, it is likely that constraints on the a lattice parameter arising from epitaxial growth would increase the barrier above our calculated value, which assumes complete relaxation of the cell dimensions. Finally, we note that our calculations are performed at 0 K, but according to Landau-Ginzburg theory, the barrier will be reduced at higher temperature.[58] Since these effects to some extent cancel, we consider the barrier calculated here to be a reasonable estimate for the actual switching barrier.

It is very informative to compare this barrier with values for other systems calculated in exactly the same manner. In bulk AlN, the calculated barrier with ss-NEB is 0.23 eV/f.u., and for a Sc$_x$Al$_{1-x}$N alloy with 20%

Sc, the calculated barrier is 0.12 eV/f.u.[29] Ferroelectric switching in $Sc_xAl_{1-x}N$ alloys has been experimentally observed at room temperature for Sc concentrations as low as 18%.[27,59] Given that our calculated barrier in LaN is significantly smaller than in the $Sc_xAl_{1-x}N$ alloy, we expect that wurtzite LaN should behave as a ferroelectric with switchable polarization.

The prospect of using LaN as a ferroelectric is somewhat tempered by the fact that its band gap is only 2.29 eV (Table I), which will lead to a smaller breakdown field than, e.g., AlN, which has a gap of 6.03 eV.[60] The low value of the calculated barrier is promising, but more work is needed to establish whether switching can be achieved before breakdown occurs.

IV. CONCLUSIONS

We have shown that YN and LaN have technologically useful properties. Both materials can crystallize in the rocksalt structure, similar to ScN, but in addition, LaN is also stable in the wurtzite structure. Rocksalt YN has an indirect band gap, while weaker p-p coupling in rocksalt LaN leads to a direct band gap. Our calculated effective masses for electrons in YN and LaN compare favorably to those of ScN, suggesting their potential usage in devices requiring high n-type conductivity.

We found that the wurtzite phase of LaN also has favorable electronic properties. The band gap is indirect, with a value of 2.29 eV, but the direct gap is only 0.18 eV higher; a "quasi-direct" band structure of this type can be favorable for applications such as in photovoltaics. We performed a thorough investigation of the polarization properties. The internal displacement parameter u=0.414 is much larger than in conventional III-nitrides. This structure leads to a smaller value of spontaneous polarization, P_{sp}=0.608 C/m^2 (referenced to the centrosymmetric layered hexagonal stucture) than in AlN, GaN, or InN; however, this smaller value actually leads to a larger polarization discontinuity at an interface with a (111) III-V zincblende compound, as we illustrated with the example of InP, which is closely lattice-matched. The predicted bound charge (0.205 C/m^2) and carrier sheet density (1.3×10^{14} e/cm^2) at the InP/LaN interface could be exploited in tunnel junctions or contact layers.

We find that wurtzite LaN has a large piezoelectric coefficient, e_{33} =1.78 C/m^2, surpassing that of AlN. The larger u parameter also renders it plausible that the polarization could be switchable, which requires moving planes of cations relative to planes of anions, with the centrosymmetric layered hexagonal structure (with u=0.5) as the barrier. Our calculated estimate for the switching barrier is 0.06 eV/f.u., significantly smaller than the value calculated in a comparable way for $Sc_xAl_{1-x}N$,[29] for which ferroelectricity has been experimentally demonstrated.[27,59]

Our results should motivate experimental efforts to synthesize YN and LaN and exploit their properties in device structures.

* American Society for Engineering Education Postdoctoral Fellow
† Author to whom to direct correspondence: vandewalle@mrl.ucsb.edu
[1] B. Biswas and B. Saha, Phys. Rev. Mater. 3, 020301 (2019).
[2] C. Zhou, A. Ghods, V. G. Saravade, P. V. Patel, K. L. Yunghans, C. Ferguson, Y. Feng, B. Kucukgok, N. Lu, and I. T. Ferguson, ECS J. Solid State Sci. Technol. 6, Q149 (2017).
[3] H. Al-Atabi, Q. Zheng, J. S. Cetnar, D. Look, D. G. Cahill, and J. H. Edgar, Appl. Phys. Lett. 116, 132103 (2020).
[4] R. Deng, B. Ozsdolay, P. Zheng, S. Khare, and D. Gall, Phys. Rev. B 91, 045104 (2015).
[5] S. Kerdsongpanya, O. Hellman, B. Sun, Y. K. Koh, J. Lu, N. Van Nong, S. I. Simak, B. Alling, and P. Eklund, Phys. Rev. B 96, 195417 (2017).
[6] N. L. Adamski, C. E. Dreyer, and C. G. Van de Walle, Appl. Phys. Lett. 115, 232103 (2019).
[7] S. Nayak, M. Baral, M. Gupta, J. Singh, M. Garbrecht, T. Ganguli, S. Shivaprasad, and B. Saha, Phys. Rev. B 99, 161117 (2019).
[8] C. P. Kempter, N. Krikorian, and J. C. McGuire, J. Phys. Chem. 61, 1237 (1957).
[9] R. Young and W. Ziegler, J. Am. Chem. Soc. 74, 5251 (1952).

[10] G. Busch, E. Kaldis, E. Schaufelberg-Teker, and P. Wachter, in *Conference Proceedings of the Colloque International du C.N.R.S. sur les Elements des Terres-Rares, Paris-Grenoble*, Vol. 1 (1970) pp. 359–373.

[11] J. Dismukes, W. Yim, J. Tietjen, and R. Novak, RCA Rev. **31**, 680 (1970).

[12] W. De La Cruz, J. Dıaz, L. Mancera, N. Takeuchi, and G. Soto, J. Phys. Chem. Solids **64**, 2273 (2003).

[13] J. M. Gregoire, S. D. Kirby, G. E. Scopelianos, F. H. Lee, and R. B. van Dover, J. Appl. Phys. **104**, 074913 (2008).

[14] L. Du, J. Edgar, R. A. Peascoe-Meisner, Y. Gong, S. Bakalova, and M. Kuball, J. Cryst. Growth **312**, 2896 (2010).

[15] J. Gregoire, S. Kirby, M. Turk, and R. Van Dover, Thin Solid Films **517**, 1607 (2009).

[16] C. Stampfl, W. Mannstadt, R. Asahi, and A. J. Freeman, Phys. Rev. B **63**, 155106 (2001).

[17] S. Zerroug, F. A. Sahraoui, and N. Bouarissa, Appl. Phys. A **97**, 345 (2009).

[18] B. Saha, T. D. Sands, and U. V. Waghmare, J. Appl. Phys. **109**, 073720 (2011).

[19] S. D. Gupta, S. K. Gupta, and P. K. Jha, Comp. Mater. Sci. **49**, 910 (2010).

[20] M. Ghezali, B. Amrani, Y. Cherchab, and N. Sekkal, Mater. Chem. Phys. **112**, 774 (2008).

[21] Y. Ciftci, K. Colakoglu, E. Deligoz, and H. Ozisik, Mater. Chem. Phys. **108**, 120 (2008).

[22] W.-C. Chen, C.-M. Lin, J. Maciejko, and C.-C. Chen, arXiv:2104.12879 [cond-mat.mtrl-sci] (2021).

[23] T.-N. Ye, S.-W. Park, Y. Lu, J. Li, M. Sasase, M. Kitano, T. Tada, and H. Hosono, Nature **583**, 391 (2020).

[24] M. Akiyama, T. Kamohara, K. Kano, A. Teshigahara, Y. Takeuchi, and N. Kawahara, Adv. Mater. **21**, 593 (2009).

[25] N. Farrer and L. Bellaiche, Phys. Rev. B **66**, 201203 (2002).

[26] H. Wang, N. Adamski, S. Mu, and C. G. Van de Walle, arXiv:2105.07325 [cond-mat.mtrl-sci] (2021).

[27] S. Fichtner, N. Wolff, F. Lofink, L. Kienle, and B. Wagner, J. Appl. Phys. **125**, 114103 (2019).

[28] N. Wolff, S. Fichtner, B. Haas, M. R. Islam, F. Niekiel, M. Kessel, O. Ambacher, C. Koch, B. Wagner, F. Lofink, and L. Kienle, J. Appl. Phys. **129**, 034103 (2021).

[29] K. H. Ye, G. Han, I. W. Yeu, C. S. Hwang, and J.-H. Choi, Phys. Status Solidi RRL , 2100009 (2021).

[30] A. Žukauskaitė, C. Tholander, J. Palisaitis, P. O. Å. Persson, V. Darakchieva, N. B. Sedrine, F. Tasnádi, B. Alling, J. Birch, and L. Hultman, J. Phys. D: Appl. Phys. **45**, 422001 (2012).

[31] P. Mayrhofer, H. Riedl, H. Euchner, M. Stöger-Pollach, P. Mayrhofer, A. Bittner, and U. Schmid, Acta Mater. **100**, 81 (2015).

[32] Y. Cherchab, B. Amrani, N. Sekkal, M. Ghezali, and K. Talbi, Physica E Low Dimens. Syst. Nanostruct. **40**, 606 (2008).

[33] B. Krause, D. S. Kuznetsov, A. E. Yakshin, S. Ibrahimkutty, T. Baumbach, and F. Bijkerk, J. Appl. Cryst. **51**, 1013 (2018).

[34] P. Hohenberg and W. Kohn, Phys. Rev. **136**, B864 (1964).

[35] W. Kohn and L. J. Sham, Phys. Rev. **140**, A1133 (1965).

[36] J. Heyd, G. E. Scuseria, and M. Ernzerhof, J. Chem. Phys. **118**, 8207 (2003).

[37] G. E. Heyd, J. Scuseria, and M. Ernzerhof, J. Chem. Phys. **124**, 219906 (2006).

[38] P. Blaha, K. Schwarz, G. K. H. Madsen, D. Kvasnicka, J. Luitz, R. Laskowski, F. Tran, and L. D. Marks, *WIEN2k, An Augmented Plane Wave + Local Orbitals Program for Calculating Crystal Properties*, edited by K. Schwarz (Technische Universität Wien, ISBN 3-9501031-1-2, 2018).

[39] P. Blaha, K. Schwarz, F. Tran, R. Laskowski, G. K. H. Madsen, and L. D. Marks, J. Chem. Phys **152**, 074101 (2020).

[40] G. Kresse and J. Furthmüller, Phys. Rev. B **54**, 11169 (1996).

[41] J. P. Perdew, K. Burke, and M. Ernzerhof, Phys. Rev. Lett. **77**, 3865 (1996).

[42] S. Mu, A. J. E. Rowberg, J. Leveillee, F. Giustino, and C. G. Van de Walle, Phys. Rev. B **104**, 075118 (2021).

[43] P. E. Blöchl, Phys. Rev. B **50**, 17953 (1994).

[44] G. Kresse and D. Joubert, Phys. Rev. B **59**, 1758 (1999).

[45] F. Tran and P. Blaha, Phys. Rev. B **83**, 235118 (2011).

[46] M. W. Chase Jr, J. Phys. Chem. Ref. Data, Monograph **9** (1998).

[47] R. Niewa, D. A. Zherebtsov, M. Kirchner, M. Schmidt, and W. Schnelle, Chem. Mater. **16**, 5445 (2004).

[48] H. A. Al-Brithen, A. R. Smith, and D. Gall, Phys. Rev. B **70**, 045303 (2004).

[49] K. Momma and F. Izumi, J. Appl. Crystal. **44**, 1272 (2011).

[50] C. E. Dreyer, A. Janotti, C. G. Van de Walle, and D. Vanderbilt, Phys. Rev. X **6**, 021038 (2016).

[51] B. J. Van Zeghbroeck, *Principles of Semiconductor Devices* (Boulder: University of Colorado, 2011).

[52] R. King-Smith and D. Vanderbilt, Phys. Rev. B **47**, 1651 (1993).

[53] R. Resta, Rev. Mod. Phys. **66**, 899 (1994).

[54] O. Madelung, U. Rössler, and M. Schulz, eds., "Indium phosphide (InP) lattice parameters, thermal expansion," in *Landolt-Börnstein - Group III Condensed Matter*, Vol. 41A1α (Springer-Verlag Berlin Heidelberg, 2001).

[55] N. L. Adamski, C. E. Dreyer, and C. G. Van de Walle, Phys. Rev. B **102**, 201301 (2020).

[56] A. Dal Corso, M. Posternak, R. Resta, and A. Baldereschi, Phys. Rev. B **50**, 10715 (1994).

[57] D. Sheppard, P. Xiao, W. Chemelewski, D. D. Johnson, and G. Henkelman, J. Chem. Phys **136**, 074103 (2012).

[58] L. Landau, Nature **138**, 840 (1936).

[59] J. Casamento, V. Gund, H. Lee, K. Nomoto, T. Maeda, B. Davaji, M. J. Asadi, J. Wright, Y.-T. Shao, D. A. Muller, A. Lal, Huili, Xing, and D. Jena, arXiv:2105.10114 [cond-mat.mtrl-sci] (2021).

[60] E. Silveira, J. Freitas, S. Schujman, and L. Schowalter, J. Cryst. Growth **310**, 4007 (2008).